Characterisation of fibre/matrix interfacial fracture energy using the single fibre peel experiment

Hottentot Cederløf, Daan Jonas; Sørensen, Bent F.

Published in:
IOP Conference Series: Materials Science and Engineering

Link to article, DOI:
10.1088/1757-899X/942/1/012029

Publication date:
2020

Document Version
Publisher's PDF, also known as Version of record

Characterisation of fibre/matrix interfacial fracture energy using the single fibre peel experiment

IOP Conf. Series: Materials Science and Engineering **942** (2020) 012029 doi:10.1088/1757-899X/942/1/012029

Characterisation of fibre/matrix interfacial fracture energy using the single fibre peel experiment

Daan J Hottentot Cederløf and Bent F Sørensen

DTU Wind Energy, Technical University of Denmark, Risø Campus, 4000 Roskilde, Denmark

E-mail: dace@dtu.dk

Abstract. An experimental method for determining the interfacial fracture energy of a single fibre undergoing peeling is presented. Peeling of a partially embedded single fibre is observed under scanning electron microscopy. The fracture energy of the fibre/matrix interface is determined by analysis of the measured curvature of the fibre near the crack tip. This study serves as a demonstration of concept for the characterization of fibre/matrix interfaces through the single fibre peel experiment. A glass fibre/vinylester interface is used as an initial test case, from which obtained interfacial fracture energies was found to be in the range from $2\,\mathrm{Jm}^{-2}$ to $14\,\mathrm{Jm}^{-2}$.

1. Introduction

The utilization of fibre reinforced polymer (FRP) composites is widespread in industries such as aerospace, automotive and wind energy. FRP composites are made up of long aligned fibres which provide high strength and stiffness, whereas the polymer (referred to as matrix) serves to protect and support the fibres. The ability to tailor component properties by controlling the fibre orientation, combined with high specific stiffness and strength in the fibre direction, means that lightweight structures may be realised. However, the out-of-plane and transverse properties are inferior in comparison with the properties in the fibre direction.

Delamination is a typical out-of-plane damage mechanism observed in composite structures, where cracks propagate in-between layers of fibres. Propagation of delamination cracks can cause loss of structural stiffness and lead to structural failure [1, 2]. Delamination growth however may be slowed, or even arrested, by fibre bridging; a phenomenon where single fibres, or ligaments of fibres, cross over between the two delaminating surfaces [3]. As the bridging fibres strain they transfer tractions between the crack faces and act as an energy absorbing (toughening) mechanism, reducing the delamination crack growth rate [4, 5]. However, this toughening mechanism is not fully understood or controlled at the micro-mechanical level, meaning it cannot be reliably incorporated during design of critical composite structures. In the case of fibre bridging under delamination, the peeling fracture energy of the fibre/matrix interface is expected to be a factor governing whether a bridging fibre breaks, or stays intact and acts as an energy absorbing mechanism [3]. It is thus of great importance to be able to characterize the mechanical properties of fibre/matrix interfaces.

Numerical modelling of fibre bridging in wood was demonstrated by Mirzaei et al. [6]. Bridging elements (single fibres and ligaments of fibres) were modelled as cross linking beams. Mirzaei et al. mentioned briefly that if the fibre was only slightly embedded that a peeling

action would be a source of energy dissipation and thus a peeling fracture energy is needed. A reference is made to the work by Kinloch et al. ([7]), with no further explanation for how such a fibre/matrix peeling fracture energy value is to be obtained. Kinloch et al. [7] studied the adhesive fracture energy of peeling flexible laminates. By accounting for internal strain energy, energy dissipated by bending and tensile deformation, they determined the geometry independent fracture energy of the interface between the peeling arm and substrate. This was concluded to be a material specific property due to the insensitivity to geometry, however its scope is limited to laminae interfaces.

1.1. Background and Motivation

The interface between the fibre and matrix is one of the most critical aspects of composite materials. Interfacial properties are controlled by the *size* (or *sizing*); a surface coating applied to the fibre during production [8]. Sizing is applied to glass fibres to facilitate bonding the fibre with a specific resin type [8]. Given the fact that size formulae are closely guarded industry secrets and that no test standards exist, the fibre matrix interface remains one of the least understood aspects of composite materials [8, 9].

Existing micro-mechanical experiments, related to the fibre/matrix interface, focus on the shearing between fibre and matrix, in some form of pull-out or push-out of the fibre ([10, 11]. However, stress concentrations, full circumferential fibre/matrix contact and fibre/matrix friction may give erroneous results [12]. At the very least they present significant challenges when pursuing a pure interfacial fracture energy because two processes are occurring at the interface simultaneously; debonding (fracture) and frictional sliding. In the debonding process, chemical bonds are broken at the fibre/matrix interface (fracture energy measured in Jm^{-2}) whereas in the sliding process shear stress (measured in Nm^{-2}) is introduced due to friction [10]. As evidence of the difficulty of isolating these two parameters: three different studies (using either analytical or numerical models) of the same test data (single fibre fragmentation test of glass/epoxy [13]) resulted in three different interfacial fracture energies: $120\,\mathrm{Jm}^{-2}$ [13], $12\,\mathrm{Jm}^{-2}$ [14] and $27\,\mathrm{Jm}^{-2}$ [10]. Furthermore, these shear based experiments are not applicable in the case of fibre bridging where fibres are exposed to both peeling and pulling.

A single fibre peel test was proposed by Alimuddin and Piggott [12] to determine the fracture energy of a fibre/matrix interface. Fibres (glass, carbon and aramid) were placed in resin that had gelled so that they sank to approximately half their diameter. After curing the single fibres were peeled out of the resin whilst placed on a microbalance that allowed both force and displacement to be measured. These measurements were used to calculate the fracture energy for the fibre/matrix interface. The fracture energy was determined to be $140 \pm 50\,\mathrm{Jm}^{-2}$ for the glass/epoxy interface of a 22 µm thick fibre. The testing of carbon/epoxy and aramid/epoxy interfaces resulted in fracture energies of $60 \pm 20\,\mathrm{Jm}^{-2}$ and $250 \pm 40\,\mathrm{Jm}^{-2}$, respectively. It was noted that the aramid fibre showed fibrilation, i.e. the fibre itself experienced splitting, which would contribute to the higher apparent fracture energy of $250 \pm 40\,\mathrm{Jm}^{-2}$. Furthermore, fibres of all three types may have been overembedded in the epoxy resin, which could increase the apparent fracture energy due to plastic deformation in the resin covering the fibre sides.

Liechti and Chai [15] performed mixed mode fracture mechanics experiments on pure glass/epoxy interfaces at different phase angles. The phase angle, ψ, is related to the complex stress intensity factor used in linear elastic fracture mechanics of interfaces, see Rice [16] and Hutchinson and Suo [17]. In the case of interface cracks, the crack tip stress field does not separate into pure normal (Mode I) and tangential (Mode II) fields. In simplified terms, a phase angle of around 0 degrees indicates a predominantly normal opening whereas a phase angle of 90 degrees indicates a predominantly tangential opening at the crack tip. Liechti and Chai found interfacial fracture energies ranging from 4 to $36\,\mathrm{Jm}^{-2}$ for $-50 < \psi < 88$ deg, respectively. They noted that for $0 < \psi < 45$ deg the fracture energy is relatively independent of mode mixity.

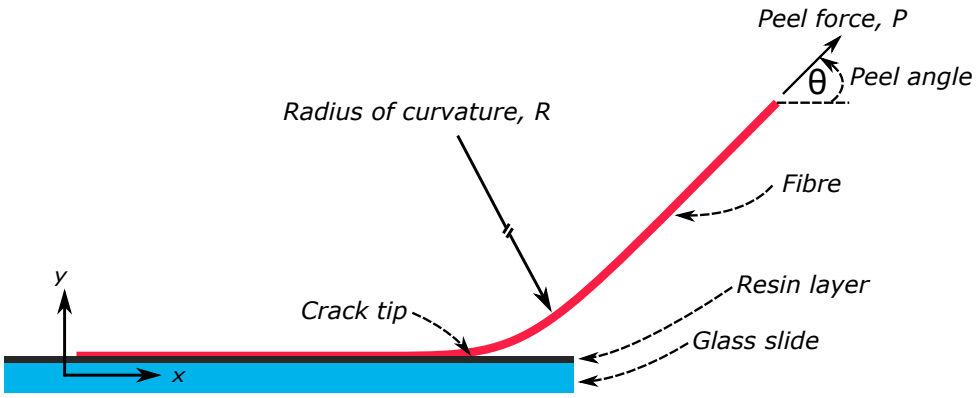

Figure 1: Illustration of test specimen.

An interesting finding by Kinloch et al. [7] observed that the mode-mixity near the crack front of thin films under peel is similarly insensitive to the applied peeling angle. This is further supported by Thouless and Jensen [18] who found that the phase angle for a thin films, with high stiffness, undergoing delamination (peel) is relatively insensitive to the peel angle. The phase angle reported by Thouless and Jensen remained constant at -37.9 deg for all peel angles, which lies in the range of phase angles described by Liechti and Chai [15] where fracture energy is insensitive to mode mixity.

McDaniel et al. [19] utilized a single fibre peel experiment to study the splitting of single ultra high molecular weight polyethylene (UHMWPE) fibres i.e. the fibre itself is split in two. Their sample preparation included partially embedding single fibres onto glass slide spin-coated with epoxy. An energy balance method, inspired by the work of Kinloch et al. [7] was used to determine the fracture energy of a splitting fibre under different fracture modes. The fibre matrix interface was however not explored.

Kawashita et al. [20] developed a method that uses image analysis to derive the radius of curvature and the root rotation angle of a laminate undergoing peel. Laminate arms with thickness in the order of 1 mm were investigated using high quality digital photography. This is several orders of magnitude greater than a single glass fibre with a diameter in the order of 17 µm. Resulting fracture energy values (obtained by global energy analysis similar to Kinloch et al. [7]) were in good agreement with their analytical results.

The present paper presents a novel, scaled down adaptation of the experimental method shown by Kawashita et al. [20] by analyzing the peeling of a single fibre inside a scanning electron microscope (SEM). The general idea of the single fibre peel experiment is shown in fig. 1. A single fibre is peeled with peel force, P, at an angle, θ. The fibre/matrix interfacial fracture energy is determined by measuring the curvature of the fibre near the crack tip. This experiment may be used as a means of validating fibre bridging models or to serve as a screening tool for fibre/matrix adhesion.

2. Method

2.1. Materials

Samples were prepared by spin-coating a glass microscope slide (25x75 mm) with approximately 1 ml commercial vinyl ester resin (VE-1260, Polynt Composites UK Ltd., Stallingborough, UK). The sample preparation was performed at the University of Strathclyde [21]. The spin coater (WS-650-23 Spin Coater, Laurell Technologies Corp., city of purchase, USA) was operated at 9000 RPM for a duration of 30−50 s to obtain a resin layer thickness (H_r) of 8 µm, approximately equal to the fibre radius, r, (see fig. 2). The device was accelerated to operating rotational speed

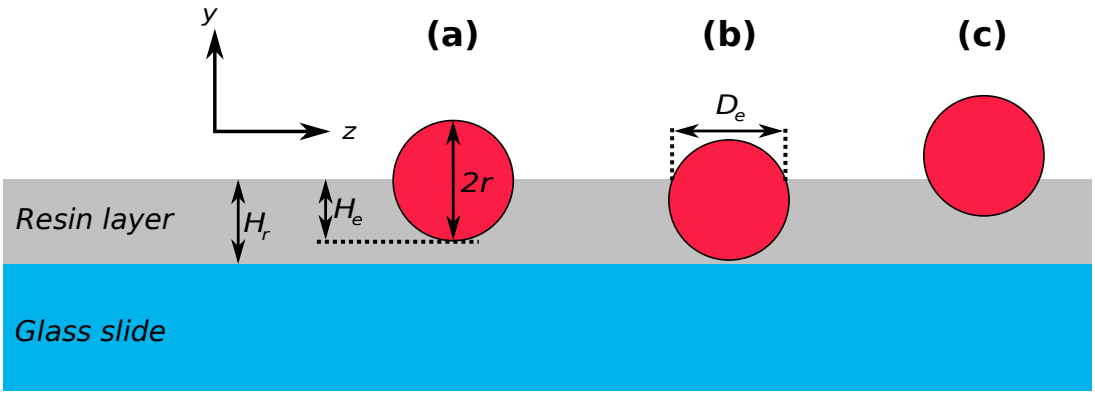

Figure 2: Illustration of test specimen cross section showing three levels of 'embeddedness': (a) fibre embedded to a height (H_e) of exactly its radius; (b) an over-embedded fibre; (c) an under-embedded fibre. The terms H_r and H_e refer to the resin height and the embedded height/depth of the fibre, respectively. The term D_e is the visible diameter when looking onto the fibre from a top view perspective (i.e. in the $x-z$ plane).

in 10 s and decelerated within 2−3 s. Commercial sized glass fibres (SE3030, 3B Fibreglass sprl., Battice, Belgium) with diameter 16−18 µm were hand placed onto the spin-coated microscope slide and cured according to supplier specifications. Final specimens were obtained by cutting the microscope slide to fit in the SEM fixture and sputter coating with gold (ca. 7 nm layer thickness).

2.2. Experimental setup

Specimens were tested and observed inside a scanning electron microscope (SEM) (EVO 60, Carl Zeiss A.G., Oberkochen, Germany) whilst mounted to a custom made fixture with a movable stage, as shown in fig. 3. The movable stage is actuated by a fine thread shaft which in turn is driven by a stepper motor. This results in a precise and accurate displacement control of the movable stage with roughly 100000 steps per mm of stage displacement. In order to observe the crack tip, the fixed and movable stages were tilted at an angle of $\varphi = 10°$ with respect to the electron beam originating from the LaB_6 filament (SEM gun), see fig. 3. This ensures that the edge of the microscope slide and any unevenness in the vinyl ester resin layer do not hide the embedded section of the fibre.

The SEM was operated at an accelerating voltage of 15 kV and a working distance of 10 mm. In order to capture a frame as close to the occurrence of fracture as possible every scan of the SEM was saved in a video recording. By employing a high scan speed with minimal noise reduction a frame rate of 2-2.5 frames per second was achieved.

2.3. Video analysis

A Matlab [22] script was prepared to extract and analyze still frames from the SEM video. After filtering and binarization, the top edge of the deformed fibre is extracted as a series of (x,y) coordinates. The deflection of the fibre was fitted in three parts: a straight line (the embedded part), a curved line and a straight line away from the detachment point. In fig. 4 these are labelled: linear fit embedded, non-linear fit and linear fit detached, respectively. The lower and upper bound of the non-linear fit are determined by the residuals of the two linear fits. The bounds are defined as the point where the residual (the distance between the fitted curve and the fibre edge) of the linear fit exceeds 1 µm. Note that the lower bound is not the same as the crack tip location. The x co-ordinate of the crack tip location is determined by visual inspection

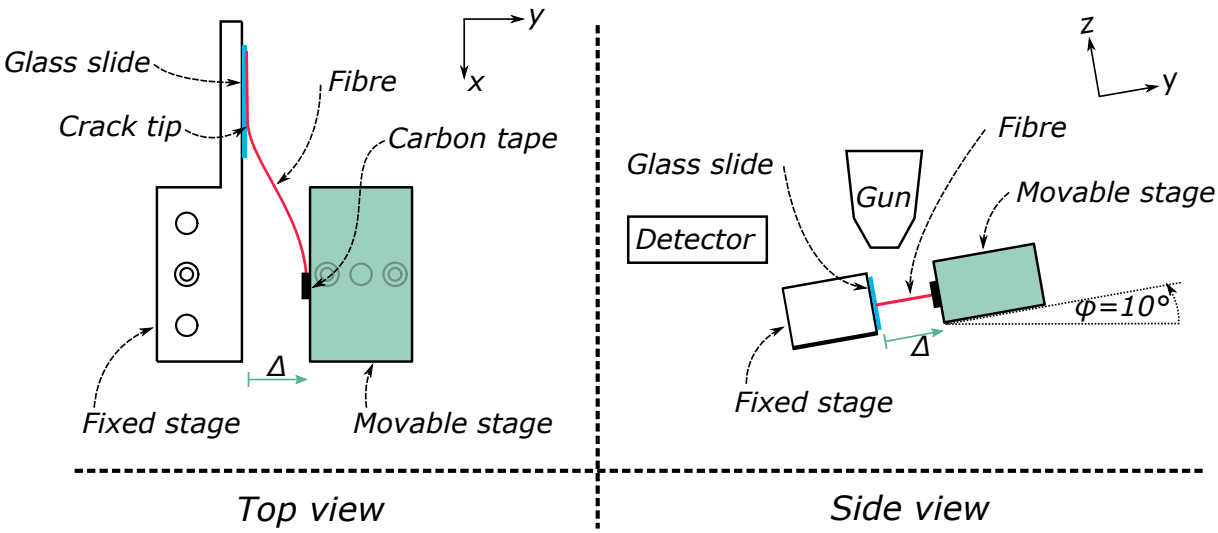

Figure 3: Illustration of test setup in the SEM. The top view is the view from the SEM gun. The movable stage translates in the y-direction a displacement Δ to peel the fibre from the glass slide mounted on the fixed stage.

of SEM images. Kawashita et al. [20] proposed an alternative method with a piecewise linear fit, this however requires extensive smoothing of the obtained fibre edge coordinates. The radius of curvature in the non-linear segment is obtained from differential geometry (eq. (1)) [23]. A detailed description of the image analysis method is detailed in the appendix.

$$\frac{1}{R(x)} = \frac{|y''(x))|}{[1 + (y'(x))^2)]^{\frac{3}{2}}} \tag{1}$$

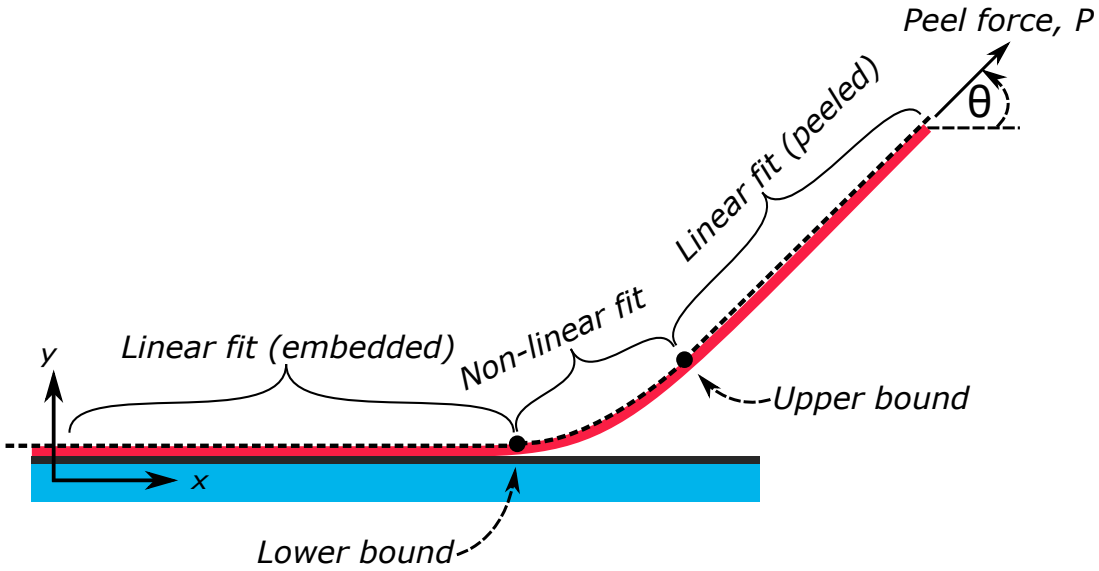

Figure 4: Illustration of the fitting procedure of the top edge of the fibre.

2.4. Fracture energy analysis

The fracture energy is determined by the curvature of the single fibre near the crack tip, the fibre modulus, E, and the fibre radius, r.

We start with the energy release of a beam under pure moments determined by the J-integral as given by [24]

$$J = \frac{M^2}{2BEI} \tag{2}$$

where M and B are the moment at the crack tip and beam width, respectively, E and I are the Young's modulus and second moment of area. In the case of the a single fibre the beam width is equal to two times the fibre radius, r (eq. (3)).

$$B = 2r \tag{3}$$

The second moment of area for a circular cross section is given by

$$I = \frac{1}{4}\pi r^4 \tag{4}$$

From classical beam theory [25] we obtain the relation between moment, M, and beam radius of curvature, R:

$$M = \frac{EI}{R} \tag{5}$$

Finally, we assume that the increase in fracture area to be the product of half the fibre circumference and the incremental crack growth, da, as shown in eq. (6). This implies that the embedded depth (H_e in fig. 2) is equal to the fibre radius. The validity of this assumption may be checked by microscopy of the substrate after complete peeling off of the fibre or by viewing the fibre from a top view ($x-z$ plane) prior to peeling to check how deep the fibre is embedded. The measurement of 'embeddedness' prior to peeling is demonstrated in fig. 5.

$$dA = \pi r da \tag{6}$$

We may then set the energy release to be equal to the energy consumed over a small crack growth, resulting in the relationship given by eq. (7), where G_c is the fracture energy.

$$JBda = \pi G_c r da \tag{7}$$

Isolating G_c in eq. (7) and inserting eqs. (2) and (3) gives eq. (8):

$$G_c = \frac{M^2}{2\pi r EI} \tag{8}$$

Further insertion of eqs. (4) and (5) into eq. (8) results in a solution for G_c purely in terms of fibre modulus, fibre radius and the radius of curvature, as given by eq. (9):

$$G_c = \frac{Er^3}{8R^2} \tag{9}$$

Table 1: Curvature and fracture energy results from single fibre peel analysis. An elastic modulus of 70 GPa was used to calculate the fracture energy (see eq. (9)).

Sample	Meas. No.	Radius of curvature R [m]	Fibre radius r [µm]	Fracture energy G_c [Jm^{-2}]
S3-02	1	7E-04	8.1	9
S3-02	2	6E-04	8.1	14
S3-02	3	8E-04	8.1	8
S3-03	4	12E-04	8.1	3
S3-03	5	14E-04	8.1	2

3. Results and observations

Two samples of SE3030/VE1260 were successfully tested in the SEM. The measured radii of curvature and calculated interfacial fracture energy are presented in table 1. It was possible to obtain multiple measurements from the same specimen. The data points in table 1 were taken from the frame before fracture occurred.

In fig. 5 a top view is presented of a single embedded fibre (specimen S7-03) and the same fibre un-embedded ca. 10 mm away. Measurement of the visible fibre diameter (16.7 µm) and measurement of the same fibre un-embedded 17.4 µm are indicated. The visible fibre diameter of the embedded portion of the fibre is 0.7 µm smaller showing that the fibre in this section was overembedded ($H_e > r$ in fig. 2) by 4% of the fibre diameter.

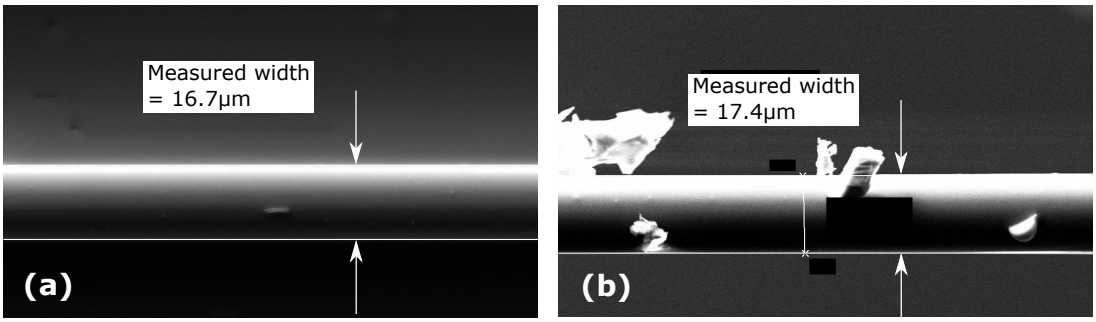

Figure 5: Top view ($x - z$ plane) width measurement of sample S7-03 (not tested in peel). **(a)** Measurement of the un-embedded fibre shows a fibre diameter, $2r$, of 17.4 µm. **(b)** Measurement of the same fibre embedded in resin shows a visible diameter (D_e) of 16.7 µm indicating that the fibre here is over-embedded (i.e. $H_e > r$ in fig. 2).

4. Discussion

Preliminary results show the feasibility of sample preparation and in-situ SEM observation of a single fibre undergoing peeling. However, a large scatter in the limited number of results are observed; between the two samples and between the measurements of the same sample. A lower radius of curvature (i.e. higher interfacial fracture energy) was systematically observed for sample S3-02 than for S3-03.

It is possible that the fibre 'embeddedness' is varying causing a measurable difference in fracture energy. If the fibre is over-embedded, the failure mode changes from a pure peeling action to also include elastic (and possibly plastic) shearing of the overlaying matrix, increasing the energy required to peel out the fibre. Sample S7-03 was checked for embeddedness, it was found that 96% of the fibre was visible. In comparison with the 'embeddedness' of up to 40%

reported by Alimuddin and Piggott [12], this is deemed acceptable. Future peel experiments must be initiated with an analysis of embeddedness prior to mechanical testing to ensure that the assumption of a perfectly half-embedded fibre holds.

The fracture energies obtained (between 2-14 Jm^{-2}) are comparable to the mode I fracture energy values measured by Liechti and Chai (ca. 4 Jm^{-2}) [15] for glass/epoxy interfaces but much lower than the fracture energy obtained by Alimuddin and Piggott for a glass/epoxy system (160 Jm^{-2}) [12]. Two factors may account for that large discrepancy. Firstly, Alimuddin and Piggott reported that their fibres were over-embedded, with down to just 60% of the fibre diameter visible. This means that as the fibre is peeled out, the matrix that sits around the top of the fibre must be plastically deformed, thereby increasing the apparent toughness. Secondly, they used epoxy resin systems which are generally a tougher matrix system than vinyl ester [26, 27].

Several challenges present themselves when working with in-situ testing inside a scanning electron microscope. A single high resolution image typically takes in the order of 10 or more seconds to capture. This does not allow for dynamic events such as the peeling action to be captured. Resolution and sharpness were traded in favour of framerate to obtain a maximum of 2.5 frames per second. The images obtained were sufficient to determine the radius of curvature, however it did not allow for the crack front to be accurately located. This was further influenced by the charging of the fresh fracture surface, since it was not coated with a conductive material, resulting in white spots near the crack tip.

The limited working space within the scanning electron microscope is a primary constraint for this experiment. However, possible validation data for the obtained interfacial fracture energy results could be obtained through measurement of the tensile force in the fibre, as demonstrated by Alimuddin and Piggott [12]. Furthermore, a robust method for determining the crack front must be established, with one possibility being the method described by Kawashita et al. [20] using the location of minimum radius of curvature i.e. minimum of eq. (1).

As stated in the introduction, the present paper serves as a demonstration of the concept and test setup. A much larger experimental regime is required, with different material systems, for any conclusions to be drawn on the interfacial fracture energies obtained from this test.

5. Summary

An experimental method to characterize the fracture energy of fibre/matrix interfaces is presented. This includes manufacturing of specimens, peel testing under in-situ SEM observation followed by image analysis to determine the radius of curvature of peeling fibres. The radius of curvature at the crack tip of the fibre undergoing peel is used as input in a fracture mechanics based approach to derive the interfacial fracture energy of the fibre/matrix interface. It is shown that the interfacial fracture energy may be derived using this method. However, the robustness of this technique must be explored by further experimental testing.

The experimental method presented may be utilized either as a screening method for fibre/matrix compatibility or as input for fibre bridging models which include discrete fibres undergoing bridging and peel-off. It may supplement existing micro-mechanical experiments aimed at determining the fracture mechanical properties of the fibre/matrix interface.

Acknowledgements

This research is conducted as part of the DACOMAT project. The DACOMAT project has received funding from the European Union's Horizon 2020 research and innovation programme 5 under GA No. 761072. Thanks to the research technicians: Gitte Christiansen and Jonas Heinige for preparation of the microscopy specimens. Special thanks to Erik Vogeley for patiently assisting in setup preparation, microscopy and providing sanity checks. Finally,

the collaborative work and sample preparation by DACOMAT partners at the University of Strathclyde is gratefully acknowledged.

References

[1] Overgaard L, Lund E and Thomsen O 2010 *Compos. Part A Appl. Sci. Manuf.* **41** 257–270
[2] Lee H G, Kang M G and Park J 2015 *Compos. Struct.* **133** 878–885
[3] Sørensen B F, Gamstedt E K, Østergaard R C and Goutianos S 2008 *Mech. Mater.* **40** 220–234
[4] Suo Z, Bao G and Fan B 1992 *J. Mech. Phys. Solids* **40** 1–16
[5] Yao L, Alderliesten R and Benedictus R 2016 *Compos. Struct.* **140** 125–135
[6] Mirzaei B, Sinha A and Nairn J 2016 *Compos. Sci. Technol.* **128** 65–74
[7] Kinloch A J, Lau C C and Williams J G 1994 *Int. J. Fract.* **66** 45–70
[8] Thomason J 2019 *Compos. Part A Appl. Sci. Manuf.* **127** 105619
[9] Thomason J 2020 *Polym. Test.* **85** 106421
[10] Sørensen B F 2017 *Mech. Mater.* **104** 38–48
[11] Yang L and Thomason J L 2010 *Compos. Part A Appl. Sci. Manuf.* **41** 1077–1083
[12] Alimuddin M and Piggott M 1999 *Polym. Compos.* **20** 655–663
[13] Kim B W and Nairn J A 2002 *J. Mater. Sci.* **37** 3965–3972 ISSN 00222461
[14] Graciani E, Varna J, Mantič V, Blázquez A and París F 2011 *Procedia Eng.* **10** 2478–2483 ISSN 18777058
[15] Liechti K M and Chai Y S 1992 *J. Appl. Mech. Trans. ASME* **59** 295–304 ISSN 15289036
[16] Rice J R 1988 *Am. Soc. Mech. Eng.* **55** 98–103 ISSN 04021215
[17] Hutchinson J W and Suo Z 1992 *Adv. Appl. Mech.* **29** 63–191 ISSN 0065-2156
[18] Thouless M and Jensen H 1992 *J. Adhes.* **38** 185–197
[19] McDaniel P B, Deitzel J M, Gregory D, Polakovic T and Gillespie J W 2018 *J. Appl. Polym. Sci.* **135** 1–11
[20] Kawashita L F, Moore D R and Williams J G 2005 *J. Mater. Sci.* **40** 4541–4548
[21] Jenkins P G, Bryce D, Xypolias G and Thomason J L 2020 *Proceedings of the 41st Risø international symposium on materials science*
[22] The Mathworks Inc 2018 *MATLAB (R2018b)* (Natick, Massachusetts)
[23] Stewart J 2008 *Calculus, Early Transcendentals* 6th ed (20 Davis Drive, Belmont, CA, USA: Brooks/Cole) ISBN 9780871702807
[24] Rice J R 1968 *Journal of Applied Mechanics* **35** 379
[25] Timoshenko S P and Goodier J N 1951 *Theory of Elasticity* (New York, USA: McGraw-Hill) ISBN 9780871702807
[26] Orozco R 1999 *Effects of Toughened Matrix Resins on Composite Materials for Wind Turbine Blades* Msc thesis Montana State University
[27] ASM International 1988 *Engineered Materials Handbook Vol 2: Engineering Plastics* (Materials Park, OH, USA: ASM International) ISBN 9780871702807

Appendix A. Image analysis method

In fig. A1 a flowchart is presented, giving an overview of the various steps taken in the script. Each step is detailed in the bullet list below.

- *Length conversion:* The fibre diameter is measured in pixels and converted to µm.
- *Image prep:* A frame is selected manually (one frame before debond crack propagation) and extracted from the video input. After cropping and rotating it is converted to a binary image using the ForegroundPolarity option (threshold of ca. 0.6) in the Matlab function: imbinarize.
- *Features:* The top edge of the fibre is extracted as a series of (x, y) coordinates (using the coordinate system shown in figs. 1 and 4).
- *Linear fit:* Two linear fits are made on the straight segments of the fibre as shown in fig. 4 using the matlab toolbox: cftool. Next, the upper and lower bounds for the non-linear fit (see fig. 4) are determined to be where the error of the linear fits exceeds a threshold of 1 µm.
- *Non-linear fit:* The curved section of the fibre is fitted with a quadratic function, $y(x)$, using the matlab toolbox cftool.

- *R and G_c:* From the non-linear fit parameters the radius of curvature, R, is calculated as a function of x using eq. (1), where y' and y'' are the second and first derivatives of the non-linear fitting function y.

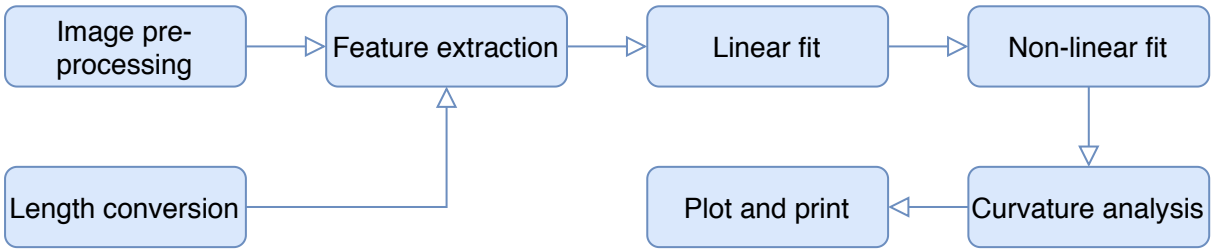

Figure A1: Flowchart of Matlab program used to perform video/image analysis.

The full Matlab code is available upon request.